ORIGINAL PAPER

Corrosion-Wear Resistance and Interfacial Morphologies of Novel Fe–Cr–B Cast Steels in Molten Aluminum

Xianman Zhang[1] · Weiping Chen[2] · Hongfeng Luo[1]

Abstract

In order to improve the corrosion–wear resistance properties of steels in molten aluminum, novel Fe–Cr–B cast steels with different boron concentrations were prepared. The steels were investigated at 750 °C for 0.5 h using a ring-block corrosion–wear test, and the interfacial morphologies were examined. Results showed that the corrosion–wear resistance of the Fe–Cr–B cast steel was three times that of H13, and benefited greatly from the effects of the primary Cr-rich Fe_2B, which bore the main load during the corrosion–wear test. The corrosion–wear behavior of the coarse primary Cr-rich Fe_2B in molten aluminum was clearly different from that in static molten aluminum.

Keywords Molten aluminum · Corrosion–wear · Fe–Cr–B cast steel · Cr-rich Fe_2B

1 Introduction

In modern industry, corrosion caused by molten metal is very common, given the need for transport and handling of molten metal. However, this corrosion is often accompanied by wear. It is known that the corrosion–wear induced by molten metal is in fact a type of mechanical–physicochemical process that involves dissolution, diffusion, reactions in solid and liquid, wear, and the interactions among them [1]; therefore, the effects will obviously differ from those that occur in most solutions, which involve a mechanical–electrochemical process [2–4]. Corrosion–wear in molten metal is one of the extreme states present in engineering processes. It is not the simple sum of corrosion and wear. When wear is added to corrosion, the two processes occur simultaneously. This results in a synergistic effect, with the worn surface altered by corrosion, while the corroded surface is altered by wear [1–5]. Among the molten metals, aluminum is the most difficult corrosion–wear problem to deal with due to its high chemical reactivity [6–9].

Since wear can occur in various forms, including erosion, abrasion, sliding and fretting, various types of corrosion–wear testing equipment is used in molten metal environments [1, 5, 10, 11]. Molten aluminum is known to produce higher temperatures and greater corrosion than other molten metals, particularly relative to molten zinc; thus there are few corrosion–wear test apparatuses for use in molten aluminum. To date, most research on corrosion–wear in molten aluminum has been carried out using stirring methods [11–13]. Yu et al. [12] found that the dissolution of H13 was faster and the intermetallic layers were thinner with higher agitation of molten aluminum, which was confirmed by other researchers [13]. Our previous work [14, 15] revealed that Fe–Cr–B cast steels were highly resistant to molten aluminum corrosion, with the Cr-rich Fe_2B playing a key role in the improved resistance. In addition, the corrosion products of Cr-rich Fe_2B were found to be periodic layered structures (PLS). In other works, Ma et al. [5, 16–19] studied the corrosion and erosion–corrosion behavior of a Fe–B alloy in molten zinc, and found that Fe_2B had a strong orientation effect on the erosion–corrosion resistance of the alloy. However, it is not known whether the corrosion–wear behavior of Cr-rich Fe_2B is the same as that of Fe_2B in molten zinc or in static molten aluminum. Therefore, in the present work, novel Fe–Cr–B cast steels containing different concentrations of B element were prepared, and

✉ Xianman Zhang
  xianman213@163.com

[1] Mechanical and Electrical Engineering College, Hainan University, Haikou 570228, Hainan Province, People's Republic of China

[2] Guangdong Key Laboratory for Advanced Metallic Materials Processing, South China University of Technology, Guangzhou 510640, Guangdong Province, People's Republic of China

their corrosion–wear resistance and interfacial morphologies in molten aluminum were investigated.

2 Experimental

2.1 Materials

The novel Fe–Cr–B cast steels were prepared by melting a mixture of clean A3 steel and ferrous alloys including Fe–70 wt% Cr, Fe–32 wt% B, Fe–55 wt% Mo, and Fe–78 wt% Mn in a 250-kg-capacity medium-frequency induction furnace. The melt was poured into a sodium silicate–CO_2 bonded sand mould at 1450 °C to obtain Y-type ingots. The test samples, with dimensions of 10 mm × 10 mm × 10 mm, were all cut from the center of the Y-type ingots by wire-electrode cutting. In addition, H13 steel was included as a reference. The chemical composition of the Fe–Cr–B cast steels and H13 steel, as analyzed by inductively coupled plasma atomic emission spectroscopy (ICP-AES), is given in Table 1.

2.2 Corrosion–Wear Tests

The apparatus for corrosion–wear tests, as shown in Fig. 1, was illustrated schematically in our previous work [1]. The friction pair is under a ring-block structure, with the ring comprising the test material and the block comprising Si_3N_4. The shaft of the Si_3N_4 holder is rotated continuously

throughout the test. Before the corrosion–wear test, the Si_3N_4 block is trimmed using special equipment. Because the crucible can be lifted to enable the friction pair to be submerged in the molten aluminum, it can be small, and only about 3 kg pure aluminum will be enough. The load is applied through a wire rope, and the direction of the force is parallel to that of the normal stress between the friction pair, so the applied force is more accurate. In the present work, the friction pair was preheated in an electric furnace with a height of about 5 cm above the Al melt for 1.5 h, which resulted in oxidation of the surface of the sample. However, the influence of oxidation on the weight loss of corrosion–wear was so small that it could be ignored. The temperature of the molten aluminum was 750 °C, monitored by a K-type thermocouple covered by a closed-end alumina tube. Two loads of 5 and 10 N and three rotation speeds of 30, 60 and 90 r/min were applied. The duration of the corrosion–wear test was 0.5 h. The samples were cut into cubes with dimensions of $10 \times 10 \times 10$ mm^3, and all sample surfaces were polished by grinding with up to 1500-grit SiC paper. Finally, after cleaning in ethanol with an ultrasonic cleaner and blow-drying, the samples were weighed with an electronic balance. It should to be noted that, under the effect of the load, the friction pair was always in close contact with each other during the test. After the test, the crucible was lowered to its original position, and the samples with residual aluminum were cooled to room temperature in air. To evaluate the weight loss and observe the worn

Table 1 The chemical compositions of Fe–Cr–Mo–B cast steels and H13 steel (wt%)

Elements	C	B	Si	Cr	Mo	Mn	Ni	V	Al	Fe
M4	0.36	2.03	1.51	13.46	2.19	6.89	0.50	0.62	0.21	Bal
M5	0.36	3.12	1.85	12.95	2.11	6.24	0.48	0.58	0.15	Bal
M6	0.36	3.64	2.19	12.38	1.89	5.88	0.44	0.56	0.12	Bal
H13	0.38	–	1.0	5.3	1.3	0.4	0.05	0.9	–	Bal

Fig. 1 High-temperature test rig for corrosion–wear in molten metal built by South China University of Technology (SCUT): 1—electromotor; 2—force-loading system; 3—furnace lifting device; 4—frame; 5—pressure sensor; 6—rotating shaft; 7—loading lever; 8—cube specimen; 9—annular friction pair (Si_3N_4); 10—furnace ; 11—molten metal; 12—crucible; 13—sample clamp
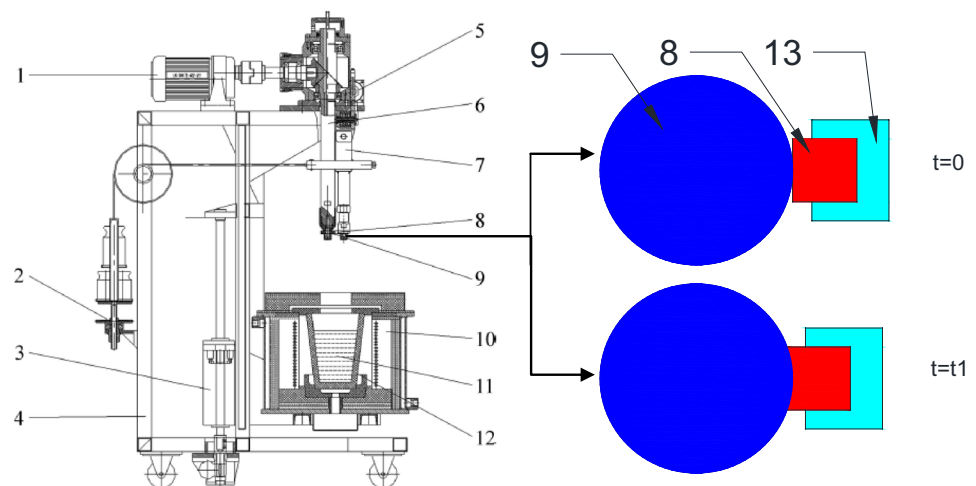
surface morphology (top view), some of the corrosion–wear specimens of the Fe–Cr–B cast steels were placed in a 10% NaOH solution to remove the residual aluminum. The calculation of weight loss directly characterized the corresponding properties. The specimens with residual aluminum were cut perpendicularly to the solid/liquid interface for cross-sectional metallographic examination using standard grinding and polishing. The microstructure of each specimen was observed under a Zeiss Supra 40 (Carl Zeiss NTS GmbH, Germany) scanning electron microscope (SEM) with backscattered electron (BSE) and secondary electron (SE) modes. The chemical line profiles from the surface were investigated using a field emission electron probe microanalyzer (Jeol JXA-8530F; Shimadzu, Japan).

3 Results and Discussion

### 3.1 As-Cast Microstructure of Fe–Cr–B Cast Steel

Figure 2 shows that the microstructures of Fe–Cr–B steels are mainly composed of a Fe dendrite metal matrix and typical eutectic network-structured M_2B-type borides (M = Cr, Mo). Coarse primary Cr-rich Fe_2B also appeared as the boron concentration increased, which was shown in our previous work as well [14, 15].

3.2 Corrosion–Wear Properties in Molten Aluminum

The weight losses of the specimens after corrosion–wear under a load of 10 N at different rotation speeds are presented in Fig. 3a. As the figure shows, the weight losses for M4–M6 were much smaller than that of H13. In addition, the weight loss increased as the rotation speed increased, although the relationship was not linear. That is to say, the Fe–Cr–B cast steels exhibited high corrosion–wear resistance in molten aluminum especially at the higher rotation speed. Among the steels, the corrosion–wear resistance of M6 was three times higher than that of H13 at 10N-60r/min. Because M6 exhibited the best results, additional corrosion–wear tests were carried out on this sample under different conditions. The results are illustrated in Fig. 3b, which shows that the weight loss for M6 is much less than that of H13 under all test conditions. An increase in weight loss for M6 is also evident as the load and rotation speed increase, but the relationship in this case also does not obey a linear law. In order to show the corrosion–wear resistance comparisons under different test conditions more intuitively, the weight losses in Fig. 3b were transformed into the weight loss ratio of M6/H13, as shown in Fig. 3c. Here, the smallest weight loss ratios for M6/H13 were 25% and 29% under a rotation speed of 90 r/min, with corresponding loads of 5 N and 10 N, respectively. This indicates that the influence of rotation speed was much greater than that of load. The stirring speed for the molten aluminum increased as the rotation speed increased. Corrosion produced by dynamic aluminum melt has been shown to be more severe than that of static aluminum melt. The intermetallics on the corroded surface are loose and porous [14], so little shear stress is needed to remove them. Once the critical shear stress is reached, a further increase in load has no additional effect on the removal effect of the porous intermetallics.

Fig. 2 SEM microstructures of Fe–Cr–B cast steels: **a** M4, **b** M5, **c** M6 (to better view the colored text in this figure, the reader is referred to the online version of this article)
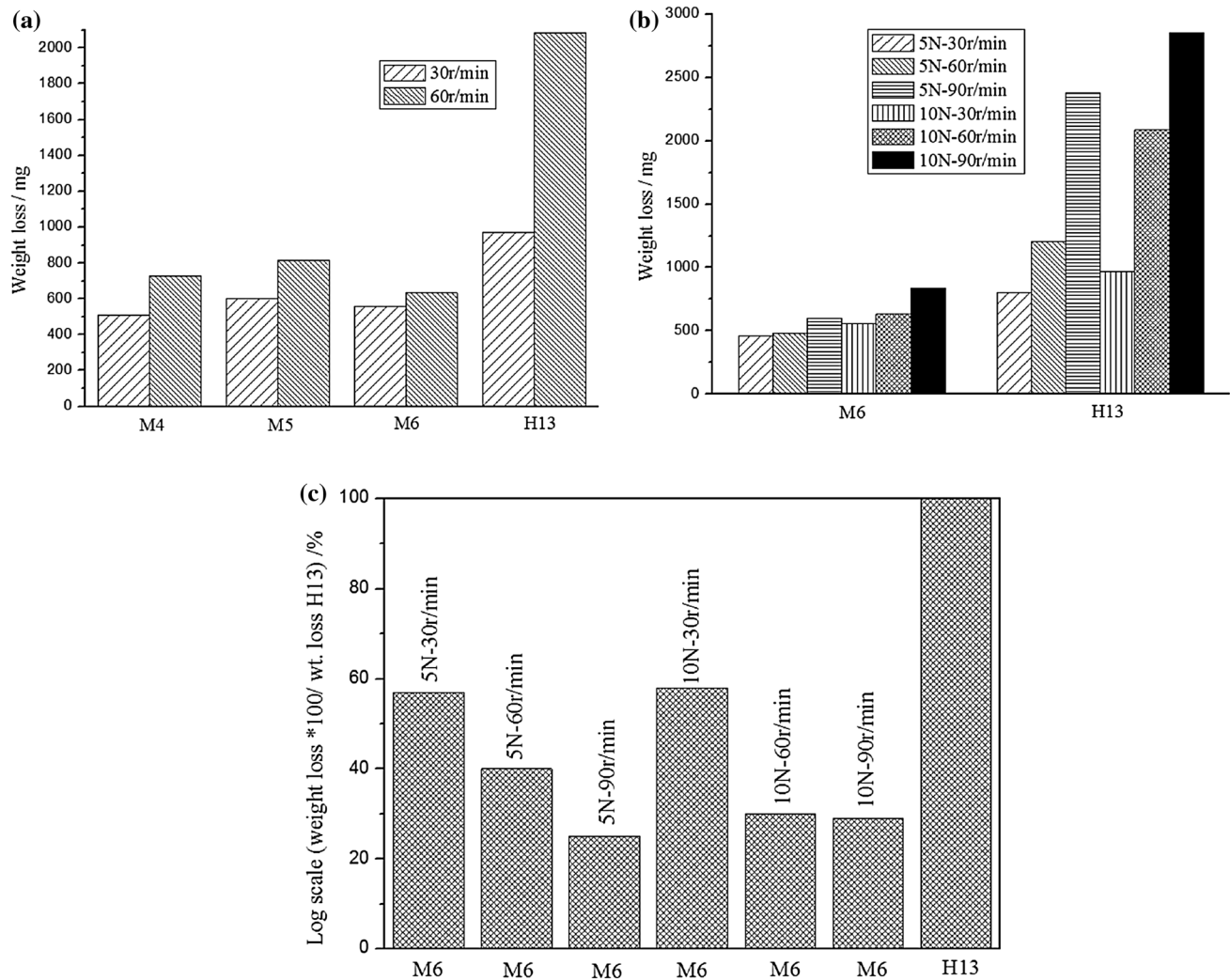
(a)

(b)

(c)
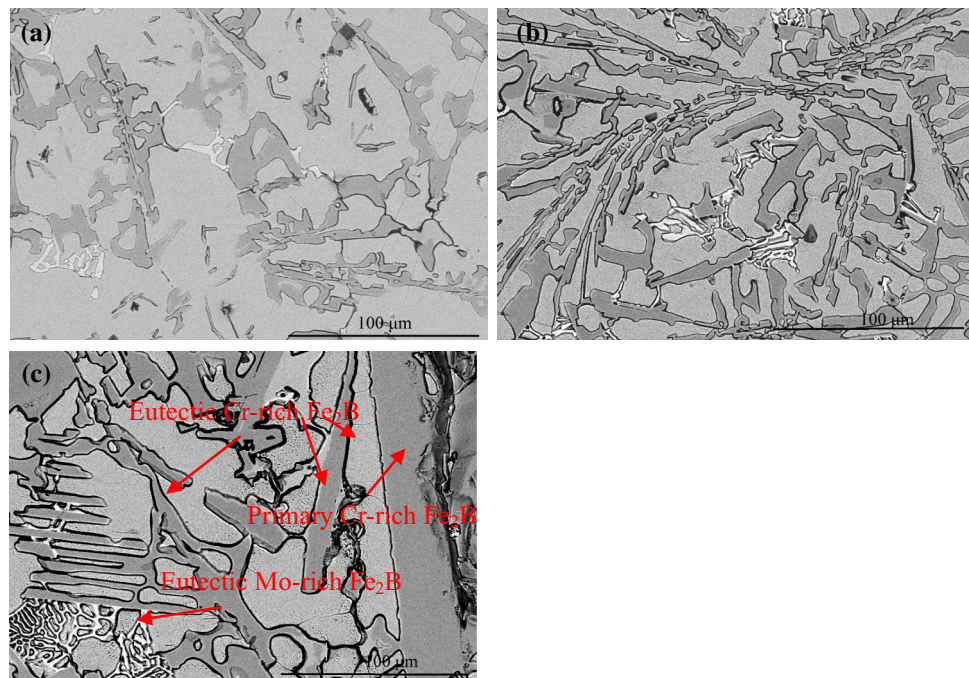
Fig. 3 Weight loss during corrosion–wear in molten aluminum under different test conditions: **a** M4–M6 and H13 under 10 N with different rotation speeds, **b** M6 and H13 under different test conditions, **c** M6 compared to H13 under different test conditions. This graph was normalized by assigning a value of 100 to H13

3.3 Microstructural Characteristics of Corrosion–Wear Samples

Figure 4a–c shows the BSE SEM images of the corrosion–wear surfaces (top view) of M6 under different test conditions. Some columnar structures (shown by arrows in Fig. 4a–d) are present on the surface, which can be attributed to the corrosion–wear products of the primary Cr-rich Fe$_2$B. Some microcracks also appear. Figure 4d shows the SE SEM image of the M6 surface under a load of 10 N and a rotation speed of 90 r/min (denoted as M6-10N-90r/min; all representations of specimens in the corrosion–wear tests were similar to this). Here it is clear that the columnar structures protrude from the surface of Fe matrix corrosion–wear products. Previous works have shown that Fe$_2$B possesses high corrosion resistance to molten aluminum [8, 14, 15]

and high wear resistance [20, 21]. Moreover, Cr has been found to improve the fracture toughness and wear resistance of Fe$_2$B [22–24]. These characteristics made the primary Cr-rich Fe$_2$B as a high corrosion–wear-resistant phase; thus they were out of the Fe matrix at the corrosion–wear interface. Consequently, the wear load was mainly applied on the coarse Cr-rich Fe$_2$B, and the Fe matrix around it primarily suffered from the corrosion of dynamic aluminum melt. In addition, the porous structure of the corrosion–wear products of the Fe matrix tended to disappear with increasing rotation speed under the same load. Therefore, the columnar structures shown in Fig. 4a–d represent the corrosion–wear products of the primary Cr-rich Fe2B, which acted as a nail to protect the products of the Fe matrix from spalling off. Thus, the better corrosion–wear resistance of M6 was due to the B element content, which resulted in the formation
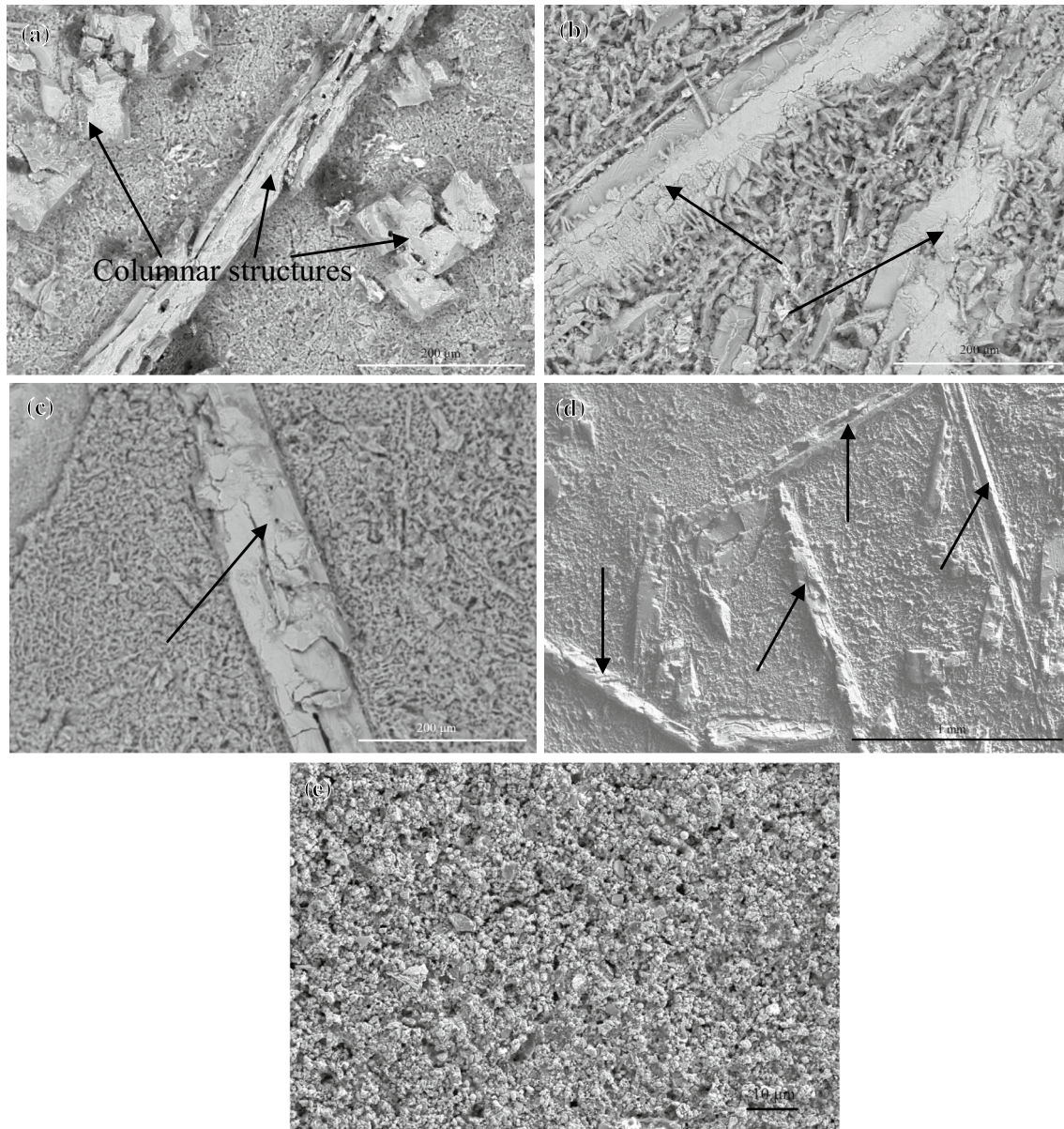
Fig. 4 Morphology of samples after the corrosion-wear in molten aluminum under different conditions: **a** M6-10N-30r/min, **b** M6-10N-60r/min, **c** M6-10N-90r/min, **d** SE mode of M6-10N-90r/min, **e** H13-10N-90r/min

of the coarse primary Cr-rich Fe_2B. Figure 4e shows the corrosion–wear surface (top view) of H13-10N-60r/min, in which no nail effect appears; thus the Fe–Al intermetallics (corrosion–wear products of the Fe matrix) were easily worn during the corrosion–wear process.

The cross-sectional morphologies of M6-10N-60r/min are shown in Fig. 5a–c. Three layers consisting of Al, intermetallics and substrate are shown, and the corrosion–wear products of coarse primary Cr-rich Fe_2B are clearly higher and protrude from the surface of the Fe matrix corrosion–wear products. The protruding portions become gray under the BSE mode, which means that some heavy metal

elements were dissolved in the molten aluminum. Microcracks exist at the tip of the protruding portions. These results are consistent with Fig. 4. The fine eutectic Cr-rich Fe_2B experienced dynamic corrosion by molten aluminum with the formation of PLS, which was due to the ability of the coarse primary Cr-rich Fe_2B to withstand the main load during the corrosion–wear process.

Figure 6 shows the elemental scanning of primary boride after corrosion–wear in molten aluminum by an electron probe micro-analyzer (EPMA) along the direction of the arrow. The gray areas of the protruding portions were found to be rich in Cr and Al, with a sharp decrease in Fe content,
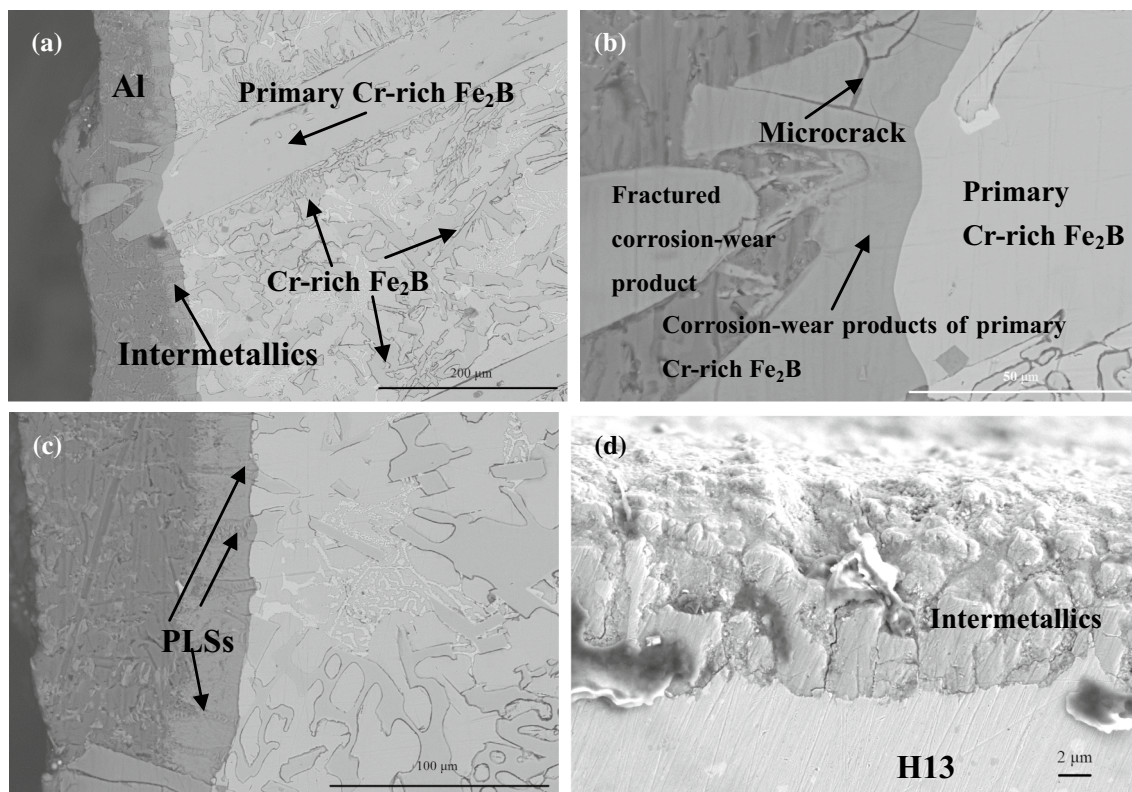
Fig. 5 Cross-sectional view of the interface of M6 and H13 after corrosion–wear in molten aluminum (750 °C, 10 N, 60 r/min, 0.5 h): **a** low magnification of M6, **b** high magnification of the primary Cr-rich Fe_2B of M6, **c** high magnification of the eutectic Cr-rich Fe_2B of M6, **d** H13

which was obviously different from the part embedded in the Fe matrix from the elemental line scan results, although the B element could not be analyzed accurately with the equipment used in this study. This is actually very difficult to detect due to its small atomic number [25–27]. The semi-quantitative composition results of the phases measured by EPMA in Fig. 6a are shown in Table 2. According to these results, most of the Fe element contained in Cr-rich Fe_2B dissolved into aluminum melt, and the Al element was diffused into the protruding portions of the Cr-rich Fe_2B during the corrosion–wear in molten aluminum, which resulted in an increase in the proportion of Cr element. The preferential dissolution of the composition of metal has been reported in the corrosion process of molten zinc as well [25, 26, 28, 29], and was dependent on the solubility in the respective metal melts.

In contrast to the cross-sectional morphologies of M6 corroded by molten aluminum for 0.5 h shown in our previous work, where PLS formed at the Cr-rich Fe_2B/Al interface [14], it was evident that PLS were formed only at the fine eutectic Cr-rich Fe_2B/Al interface during corrosion–wear. No PLS formed at the coarse primary Cr-rich Fe_2B/Al interface (as shown in Fig. 5a–c). However, the mechanisms of different behaviors of the primary Cr-rich Fe_2B during

corrosion–wear and corrosion warrant further discussion. During the corrosion–wear, aluminum melt existed between the friction pair. Wear and corrosion occurred simultaneously: the wear surface was altered by corrosion, while the corrosion surface was altered by wear. There were complex synergistic effects between corrosion and wear in molten aluminum. The aluminum melt not only acted as a lubricating film on the friction surface, but it also corroded the worn surface and accelerated the wear. Thus the phenomenon of PLS by preferential dissolution of Fe at the Cr-rich Fe_2B/ Al interface could be attributed to the fact that only a small amount of aluminum melt film existed between the friction pair under the effect of load during corrosion–wear. It was also found that the thickness of intermetallics formed during the corrosion process (about 40 μm) was much larger than that formed during the corrosion–wear process (about 25 μm) for the same test duration. These differences were attributed to the addition of wear to the process of corrosion by molten aluminum. Shear stress and agitation were the main factors causing wear.

Figure 5d shows the cross-sectional morphologies of H13-10N-60r/min; the thickness of the Fe–Al intermetallics is about 10 μm, which is clearly smaller than that formed during static corrosion for 0.5 h (about 86 μm [14, 25]). This
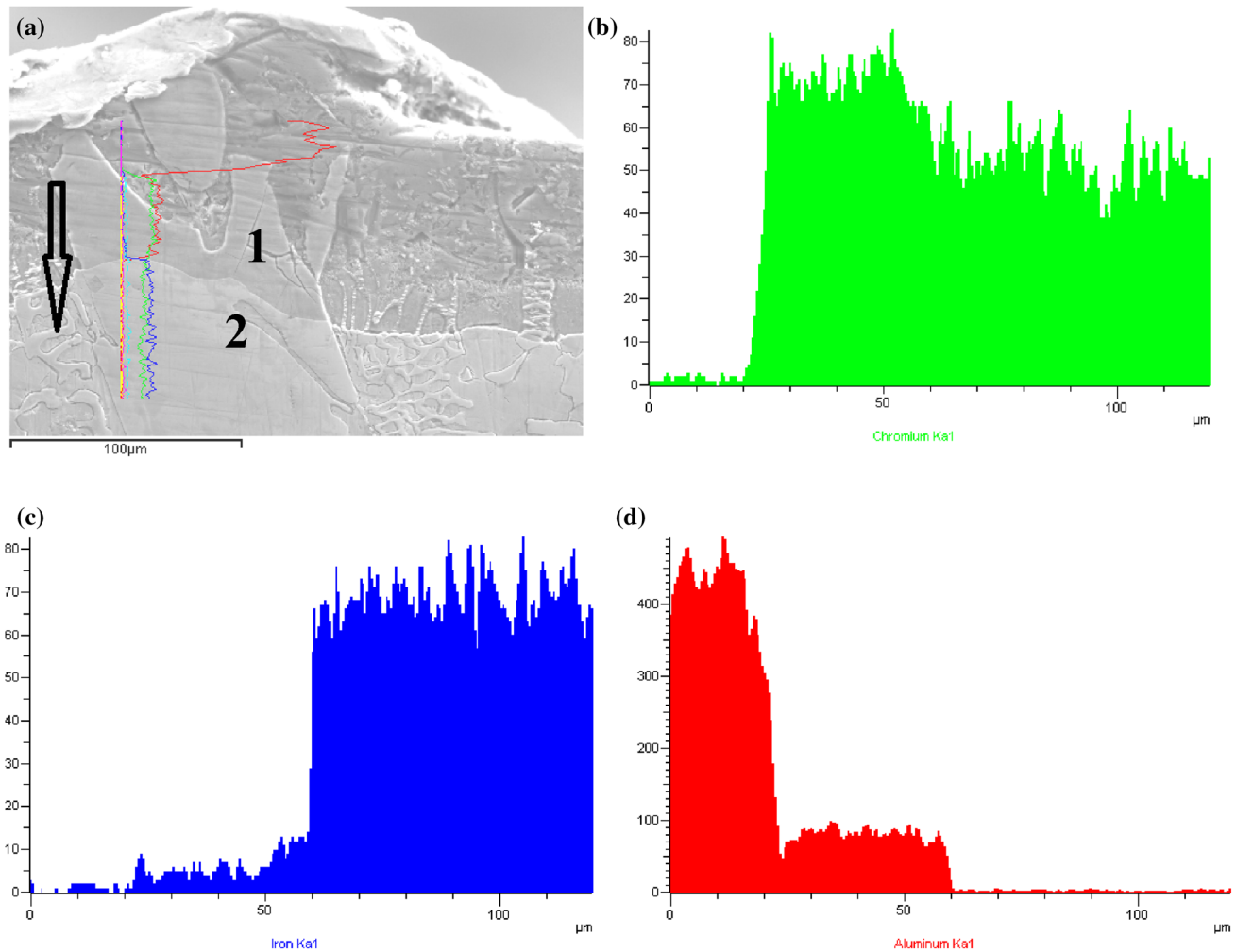
Fig. 6 Elemental scanning of primary boride after corrosion–wear in molten Al by EPMA: **a** SEM images, **b** Cr, **c** Fe, **d** Al

Table 2 Composition of the phases measured by EPMA in Fig. 6 (wt%)

Number	Fe	Cr	B	Al
1	10.6	40.6	16.8	32.0
2	62.0	30.8	7.1	0.1

result is in agreement with findings reported in the literature [12, 13]. The intermetallics/Fe substrate interface (as shown in Fig. 5d) was flatter than that formed during static corrosion for 0.5 h, shown in our previous work [30], and the saw-tooth structure was no longer evident. Compared with the interface structures of M6 shown in Fig. 5a–c, there was no protruding portion to bear the load in Fig. 5d, so the Fe–Al intermetallics were easily removed under shear stress during corrosion–wear. This is the primary reason that the corrosion–wear resistance of H13 was much poorer than that of Fe–Cr–B cast steels (as shown in Fig. 3).

In summary, Fe–Cr–B cast steels exhibited superior corrosion–wear resistance in molten aluminum. The highest resistance was shown by M6, which was three times that of H13, thus clearly benefiting from the effects of the primary Cr-rich Fe_2B. The primary Cr-rich Fe_2B, which had superior corrosion and wear resistance, protruded from the matrix, thus bearing the main load during the corrosion–wear test. It can be inferred that, during the corrosion–wear process, the corrosion of the primary Cr-rich Fe_2B caused by the molten aluminum film was not sufficient. Therefore, the Fe element in primary Cr-rich Fe_2B dissolved preferentially from the corrosion layer into liquid aluminum, accompanied by the inward diffusion of Al, resulting in the formation of intermetallics containing Cr, Al and B, which were ultimately broken under the load, while the eutectic Cr-rich Fe_2B was corroded by dynamic aluminum melt, resulting in the formation of PLS. However, further investigation of the mechanism is still needed.

4 Conclusion

Fe–Cr–Mo–B cast steels had high corrosion–wear resistance in molten aluminum compared with H13 steel. Among them, Fe–12.3 wt%, Cr-5.88 wt%, Mn-3.6 wt%, B-1.89 wt% Mo (M6) exhibited the highest corrosion–wear resistance to molten aluminum, three times that of H13. The coarse primary Cr-rich Fe_2B-type borides played an important role in improving the corrosion–wear resistance of Fe–Cr–B cast steels in molten aluminum. No PLS were formed at the primary Cr-rich Fe_2B/Al interface during corrosion–wear. The corrosion–wear behavior of the coarse primary Cr-rich Fe_2B in molten aluminum clearly differed from that in static molten aluminum.

Compliance with Ethical Standards

Conflict of interest None.

References

1. Zhang, X.M., Chen, W.P.: Review on corrosion-wear resistance performance of materials in molten aluminum and its alloys. Trans. Nonferrous Met. Soc. China **25**, 1715–1731 (2015)
2. Nourri, M., Li, D.Y.: Maximizing the benefit of aluminizing to AZ31 alloy by surface nanocrystallization for elevated resistance to wear and corrosive wear. Tribol. Int. **111**, 211–219 (2017)
3. Kkayan, N., Ghasemi, H.M., Abedini, M.: Synergistic erosion–corrosion behavior of commercially pure titanium at various impingement angles. Wear **380–381**, 154–162 (2017)
4. Zenebe, D., Yi, S., Kim, S.S.: Sliding friction and wear behavior of Fe-based bulk metallic glass in 3.5% NaCl solution. J. Mater. Sci. **47**, 1446–1451 (2012)
5. Wang, Y., Xing, J., Ma, S., Liu, G., Jia, S.: Erosion–corrosion interaction of Fe–B alloy in flowing zinc. Mater. Sci. Technol. **32**, 49–56 (2016)
6. Lou, D.C., Akselsen, O.M., Onsøien, M.I., Solberg, J.K., Berget, J.: Surface modification of steel and cast iron to improve corrosion in molten aluminum. Surf. Coat. Technol. **200**, 5282–5288 (2006)
7. Zhou, M., Li, K., Shu, D., Sun, B.D., Wang, J.: Corrosion resistance properties of enamels with high B_2O_3–P_2O_5 content to molten aluminum. Mater. Sci. Eng. A **346**, 116–121 (2003)
8. Wang, D.Q., Shi, Z.Y., Zou, L.J.: A liquid aluminum corrosion resistance surface on steel substrate. Appl. Surf. Sci. **21**, 304–311 (2003)
9. Yan, M., Fan, Z.: Review: Durability of materials in molten aluminum alloys. J. Mater. Sci. **36**, 285–295 (2001)
10. Kondo, M., Tsisar, V., Muroga, T., Nagasaka, T., Yeliseyeva, O.: Erosion–corrosion of RAFM JLF-1 steel in lithium flow induced by impeller. J. Plasma Fusion Res. Ser. **9**, 294–299 (2010)
11. Bobzin, K., Brögelmann, T., Brugnara, R.H., Kruppe, N.C.: CrN/AlN and CrN/AlN/Al_2O_3 coatings deposited by pulsed cathodic arc for aluminum die casting applications. Surf. Coat. Technol. **28**, 222–229 (2015)
12. Yu, M., Shivpuri, R., Rapp, R.A.: Effects of molten aluminum on H13 dies and coatings. J. Mater. Eng. Perform. **4**, 175–181 (1995)
13. Yang, R.F., Zhang, P., Wu, J.H.: The corrosion mechanism of a stainless steel electrode in the dynamic melting of Al at high temperature. Mater. Sci. Eng. A **499**, 134–137 (2009)
14. Zhang, X.M., Chen, W.P., Luo, H.F., Li, S., Zhou, T., Shi, L.Y.: Corrosion resistance and interfacial morphologies of novel Fe–Cr–Mo–B cast steels in molten aluminum. Corros. Sci. **125**, 20–28 (2017)
15. Zhang, X.M., Chen, W.P., Luo, H.F., Zhou, T.: Formation of periodic layered structure between novel Fe–Cr–B cast steel and molten aluminum. Scr. Mater. **130**, 288–291 (2017)
16. Liu, G.Z., Xing, J.D., Ma, S.Q., He, Y.L., Fu, H.G., Gao, Y., Wang, Y., Wang, Y.R.: Effects of erosion angle on erosion properties of Fe–B alloy in flowing liquid zinc. Metall. Mater. Trans. A **46**, 1900–1907 (2015)
17. Wang, Y., Xing, J.D., Ma, S.Q., Liu, G.Z., He, Y.L., Yang, D.X., Bai, Y.P.: Effect of Fe_2B orientation on erosion–corrosion behavior of Fe–3.5 wt% B steel in flowing zinc. Corros. Sci. **98**, 240–248 (2015)
18. Wang, Y., Xing, J.D., Ma, S.Q., Zheng, B.C., Fu, H.G., Liu, G.Z.: Interfacial morphologies and erosion–corrosion behavior of directional Fe–3.5 wt% B steel in flowing liquid Zn containing 0.3 wt% Al. Corros. Sci. **112**, 25–35 (2016)
19. Wang, Y., Xing, J.D., Ma, S.Q., Zheng, B.C., Liu, G.Z., Yang, D.X., Bai, Y.P.: Interface characterization and erosion–corrosion behavior of directional Fe–3.5 wt% B steel in flowing liquid zinc at various temperatures. Corros. Sci. **104**, 260–268 (2016)
20. Yi, D.W., Xing, J.D., Ma, S.Q., Fu, H.G., Chen, W., Li, Y.F., Yan, J.B., Zhang, J.J., Liu, Z.X., Zhu, J.: Three-body abrasive wear behavior of low carbon Fe–B cast alloy and its microstructures under different casting process. Tribol. Lett. **42**, 67–77 (2011)
21. Yi, D.W., Xing, J.D., Ma, S.Q., Fu, H.G., Li, Y.F., Chen, W., Yan, J.B., Zhang, J.J., Zhang, R.R.: Investigations on microstructures and two-body abrasive wear behavior of Fe–B cast alloy. Tribol. Lett. **45**, 427–435 (2012)
22. Ma, S.Q., Xing, J.D., Liu, G.F., Yi, D.W., Fu, H.G., Zhang, J.J., Li, Y.F.: Effect of chromium concentration on microstructure and properties of Fe–3.5B alloy. Mater. Sci. Eng. A **527**, 6800–6808 (2010)
23. Jian, Y.X., Huang, Z.F., Xing, J.D., Zheng, B.C., Sun, L., Liu, Y.Z., Liu, Y.M.: Effect of improving Fe_2B toughness by chromium addition on the two-body abrasive wear behavior of Fe–3.0 wt% B cast alloy. Tribol. Int. **101**, 331–339 (2016)
24. Jian, Y.X., Huang, Z.F., Xing, J.D., Liu, X.T., Sun, L., Zheng, B.C., Wang, Y.: Investigation on two-body abrasive wear behavior and mechanism of Fe–3.0 wt% B cast alloy with different chromium content. Wear **362–363**, 68–77 (2016)
25. Ma, S.Q., Xing, J.D., Fu, H.G., Yi, D.W., Zhang, J.J., Li, Y.F., Zhang, Z.Y., Zhu, B.J., Ma, S.C.: Interfacial morphology and corrosion resistance of Fe–B cast steel containing chromium and nickel in liquid zinc. Corros. Sci. **53**, 2826–2834 (2011)
26. Ma, S.Q., Xing, J.D., Yi, D.W., Fu, H.G., Zhang, J.J., Li, Y.F., Zhang, Z.Y., Liu, G.F., Zhu, B.J.: Effects of chromium addition on corrosion resistance of Fe–3.5B alloy in liquid zinc. Surf. Coat. Technol. **205**, 4902–4909 (2011)
27. Rai, A.K., Vijayashanthi, N., Tripathy, H., Hajra, R.N., Raju, S., Murugesan, S., Saroja, S.: Investigation of diffusional interaction between P91 grade ferritic steel and Fe–15 wt% B alloy and study

of kinetics of boride formation at high temperature. J. Nucl. Mater. **495**, 58–66 (2017)

28. Wang, W.J., Lin, J.P., Wang, Y., Chen, G.L.: The corrosion of intermetallic alloys in liquid zinc. J. Alloys Compd. **428**, 237–243 (2007)

29. Wang, W.J., Lin, J.P., Wang, Y., Chen, G.L.: The corrosion of Fe$_3$Al alloy in liquid zinc. Corros. Sci. **49**, 1340–1349 (2007)

30. Zhang, X.M., Li, X.M., Chen, W.P.: Interfacial reactions of duplex stainless steels with molten aluminum. Surf. Interface Anal. **47**, 648–656 (2015)